

## Electronic Supplementary Information for

### Gold-clay nanocomposites colloids with liquid-crystalline and plasmonic properties

Karin El Rifaii, Patrick Davidson, Laurent Michot and Cyrille Hamon

#### 1. Materials and Methods

##### 1.1. Materials

Hydrogen tetrachloroaurate trihydrate ( $\text{HAuCl}_4 \cdot 3\text{H}_2\text{O}$ ,  $\geq 99.9\%$ ) and L-Ascorbic Acid (AA, 99%) were purchased from Sigma-Aldrich. All products were used as received. Milli-Q water (resistivity 18  $\text{M}\Omega \cdot \text{cm}$ ) was used in all experiments.

##### 1.1.1. Beidellite clay preparation procedure

Natural beidellite from Idaho was purchased from the Source Clay repository from the Clay Minerals Society. The starting material was gently ground in an agate mortar and 200 g of the resulting powder were mixed with 5 liters of NaCl 1M solution. After overnight stirring, the supernatant was removed and two more conditioning steps in 5 liters of NaCl 1M solution were carried out. The resulting suspension was then placed in dialysis membranes that were placed in large excess of deionized water. The external solution was replaced until the conductivity of the bath was lower than  $20 \mu\text{S} \cdot \text{m}^{-1}$ . The content of the dialysis bag was then placed in 1 liter Imhoff cones overnight and the sedimented impurities were discarded. The final suspensions were then centrifuged in a sequential way at 5000 g, 12000 g and 35000 g. The bottom fraction of each centrifugation was redispersed in Milli-Q water to reach a concentration around 10 g/L. In the present work, only the smallest size fraction of beidellite was used and, when needed, the initial suspensions were either concentrated by osmotic stress against PEG 20000 g/mol or diluted in Milli-Q water to reach the desired initial solid concentration.

##### 1.1.2. Gold nanoparticle synthesis

In a 4 mL flask, a given equivolume of 25 mM of  $\text{HAuCl}_4$  and 250 mM AA solutions are added in sequence to a beidellite suspension, so the molar ratio of gold and AA is kept to 10 in all syntheses. After mixing the gold solution with the beidellite suspension, AA is injected under vigorous stirring to ensure homogeneous reduction of the gold precursor in the reaction medium. Details of the concentration of  $C_{\text{beid}}$ ,  $C_{\text{gold}}$  and  $C_{\text{AA}}$  and the resulting colloidal properties are described in Table 1.

Table 1: Composition of the gold-beidellite nanocomposite samples.

Sample name	$C_{\text{beid}}$ (wt %)	$C_{\text{gold}}$ (mM)	$C_{\text{AA}}$ (mM)	Colloidal properties
1	1.61	0	0	birefringent
2	1.61	0.016	0.16	birefringent
3	1.61	0.047	0.47	biphasic
4	1.61	0.16	1.6	biphasic
5	1.61	0.47	4.7	gel
6	1.61	1.6	16	gel
7	1.34	0	0	biphasic
8	1.34	0.016	0.16	biphasic
9	1.34	0.047	0.47	biphasic
10	1.34	0.16	1.6	isotropic
11	1.34	0.47	4.7	gel
12	1.34	1.6	16	gel
13	1.07	0	0	biphasic
14	1.07	0.016	0.16	isotropic
15	1.07	0.047	0.47	isotropic
16	1.07	0.16	1.6	isotropic
17	1.07	0.47	4.7	gel
18	1.07	1.6	16	gel
19	0.81	0	0	isotropic
20	0.81	0.016	0.16	isotropic
21	0.81	0.047	0.47	isotropic
22	0.81	0.16	1.6	isotropic
23	0.81	0.47	4.7	gel
24	0.81	1.6	16	gel

## 1.2. Methods

### 1.2.1. Visual Observation of the Samples

To assess how the gold nanoparticles affect the organization of the suspensions of beidellite nanosheets, series of samples with constant  $C_{\text{beid}}$  but increasing  $C_{\text{gold}}$  were examined in natural light and between crossed polarizers. They were also photographed with an Olympus XZ-1 camera, using the flash at normal incidence.

### 1.2.2. UV-Vis absorption spectroscopy

UV-vis absorption spectra were recorded with a Cary 5000 spectrometer (Agilent) in the 300 – 1000 nm wavelength range, using the absorption spectrum of water as reference. For this purpose, all the samples were filled into 1 ml polystyrene cuvettes with 1 cm optical path.

### 1.2.3. Transmission electron microscopy

Transmission electron microscopy (TEM) was performed at IMAGIF (I2BC CNRS, Gif s/Yvette, France) using a JEOL JEM-1400 microscope operating at 80 kV. For the preparation of the samples, a 10  $\mu$ L drop of nanocomposites (20 mg.L<sup>-1</sup>) was deposited on carbon-coated grids. The drop was then partially blot with a tissue paper and dried under vacuum in a Schlenk line. Analysis of the TEM images was performed with the Fiji software.

Histograms of particle sizes were obtained by measuring typically 50 particles using the ImageJ software and the particle size distributions were fitted to a log-normal dependence:

$y = \frac{A}{\sqrt{2\pi}wx} \exp\left(-\frac{\left(\ln \frac{x}{x_c}\right)^2}{2w^2}\right)$  where  $x_c$  is the center and  $w$  is the width of the particle size distribution.

### 1.2.4. X-ray scattering experiments

Small-angle X-ray scattering (SAXS) and wide-angle X-ray scattering (WAXS) measurements were performed at the Swing beamline of the Soleil synchrotron at Saint-Aubin, France. The energy of the X-ray photons was set at 12 keV, which corresponds to a wavelength  $\lambda = 1.033$  nm. For SAXS, the sample-to-detector distance was 6226 mm, which gave access to a  $q$ -range between 0.05 and 1.0 nm<sup>-1</sup>, where  $q$  is the scattering vector modulus,  $q = (4\pi/\lambda) \sin\theta$  and  $2\theta$  is the scattering angle. For WAXS, the sample to detector distance was 508 mm, providing a  $q$ -range up to 17.6 nm<sup>-1</sup>. The detector was a EIGER-4M, with a pixel size of 150  $\mu$ m. The beam size was 215 $\times$ 80  $\mu$ m<sup>2</sup> at the sample level and the exposure time was around one second.

2-dimensional scattering patterns were recorded and the usual data correction and normalization procedures were made. Moreover, the corresponding scattered intensity,  $I(q)$ , was calculated by azimuthal averaging of the scattering patterns. The suspensions were filled

into calibrated Lindemann glass cylindrical capillaries (Glas-Technik & Konstruktion, Germany) of  $1 \pm 0.1$  mm diameter, sealed with glue, and placed in an automatic sample changer.

#### 1.2.5. Sample alignment by an electric field

To align samples by applying them an electric field, we used a home-made cell that was previously described in detail.<sup>1</sup> The colloidal suspensions were filled either into flat glass optical capillaries (VitroCom NJ, USA) of 0.1 mm thickness and 2 mm width or into the same cylindrical glass capillaries used for X-ray scattering. These capillaries were placed in a plastic cell equipped with metal electrodes used to apply an alternating current (a.c.) electric field along the capillary axis. A function generator (TTi TG2000) provided a 500 kHz sinusoidal a.c. voltage that was amplified by a Krohn-Hite (7602M) amplifier to about 125 V rms amplitude. The voltage drop through the sample glass walls is not usually more than 50%. Depending on the ionic strength of the suspension, some field screening by the mobile ionic species can occur<sup>1</sup> but it did not prevent good alignment of the nanosheet suspensions.

The electric-field cell was placed on the stage of a polarizing microscope (Olympus BX 51) to allow for the observation in polarized light of the effect of the a.c. electric field on the colloidal suspensions. Photographs of the samples were recorded with an Olympus XZ-1 camera.

## 2. Additional transmission electron microscopy images

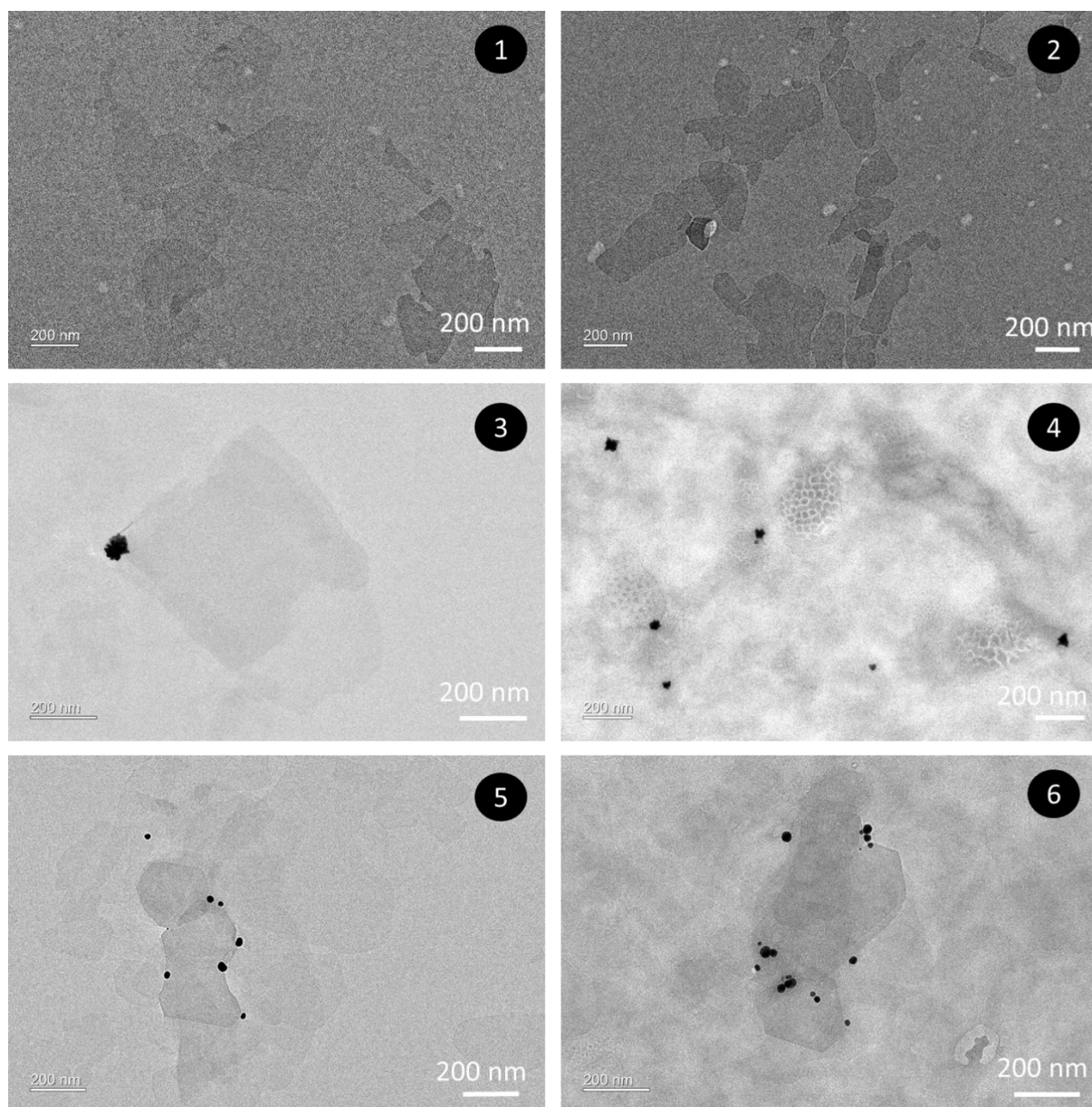


Figure S1: Representative TEM images of the samples detailed in the manuscript, denoted from 1 to 6.

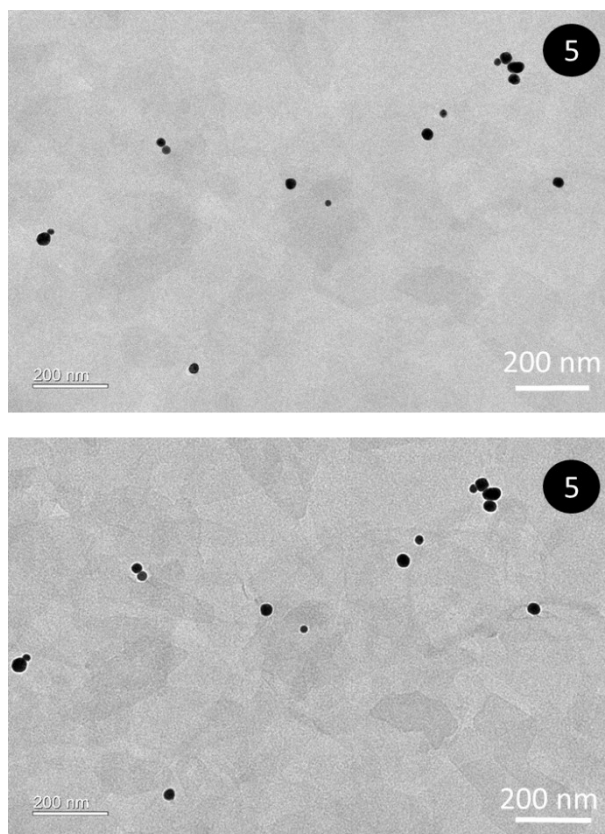


Figure S2: Two TEM images of the nanocomposite (sample 5) acquired in the same area but observed (top) in focus and (bottom) slightly under focus. Due to the high electronic contrast between gold and the beidellite nanosheets, the latter were often difficult to discern. By observing the sample underfocus, the sheets could be observed conveniently. The nanoparticles and the beidellite nanosheets were always found colocalized, suggesting a grafting of the nanoparticles on the beidellite.

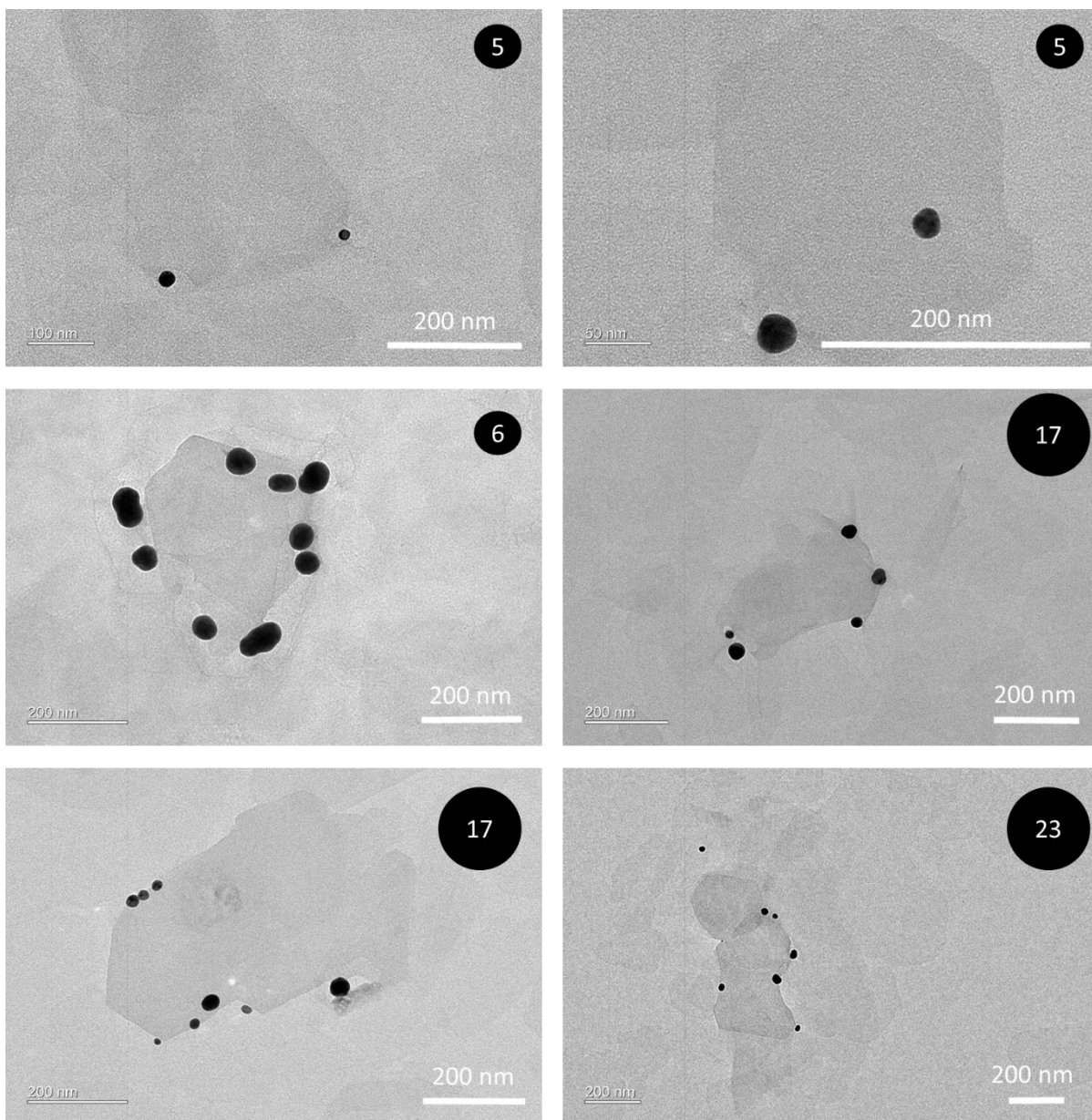


Figure S3: Additional TEM images of the samples. Nanoparticles are frequently observed at the edge of the nanosheets, suggesting that nucleation and growth of the gold nanoparticles occurs preferentially at the edge of the beidellite nanosheets.

### 3. Control samples without beidellite nanosheets

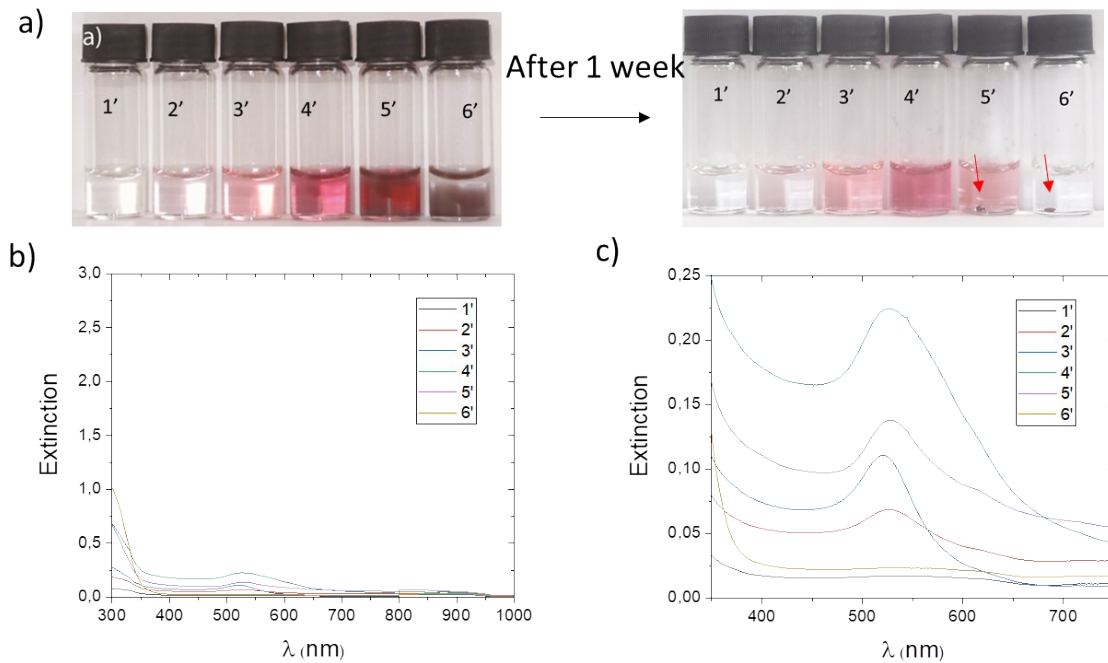


Figure S4: Optical properties of gold nanoparticles prepared without nanosheets. a) Photographs of the samples prepared in the same conditions as samples 1 to 6 (Figure 1 in the main text) but without nanosheets. 1 week after preparation, aggregation is clearly visible at the bottom of the vial, as noted by the red arrows in 5' and 6'. b) Corresponding extinction spectra. The graphs use the same scale as in Figure 1c for direct comparison. The extinction of the pure gold nanoparticle systems is significantly lower than that of the nanocomposites due to flocculation. c) Same plot as in (b) but rescaled to show the plasmon band of the sample.

#### 4. Size distributions of beidellite nanosheets and gold nanoparticles

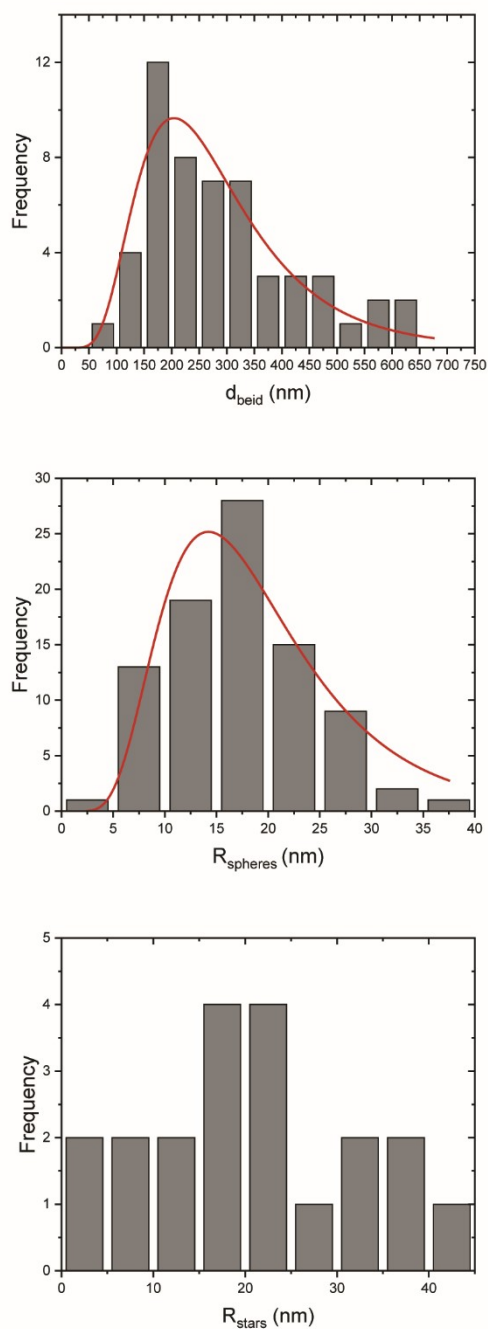


Figure S5: Size distributions of a) beidellite clay nanosheets after gold nanoparticle synthesis; b) gold nanoparticles; c) gold “stars”. In a) and b) the red curves are fits of the distributions by log-normal laws, providing  $D_{\text{beid}} = 280 \pm 140$  nm and  $R_{\text{spheres}} = 18 \pm 8$  nm. Due to the low number of particles measured, the size distribution of gold stars could not be fitted but their average radius is 21 nm. (Here, we consider the equivalent radius of a spherical particle of same projected area as the measured object.)

## 5. Effect of the ionic strength

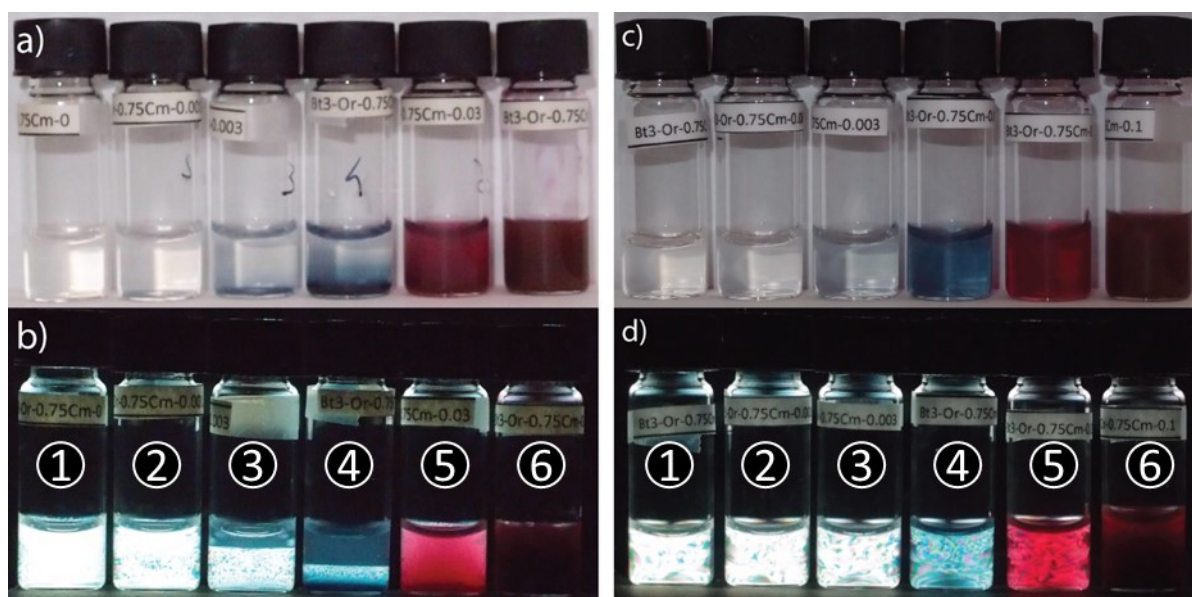


Figure S6: Photographs of the samples 1-6 before a-b) and after c-d) dialysis against deionized water observed in natural a, c) and b, d) polarized light.

## 6. Sketch of the phase diagram of the beidellite/gold nanosheet aqueous suspensions

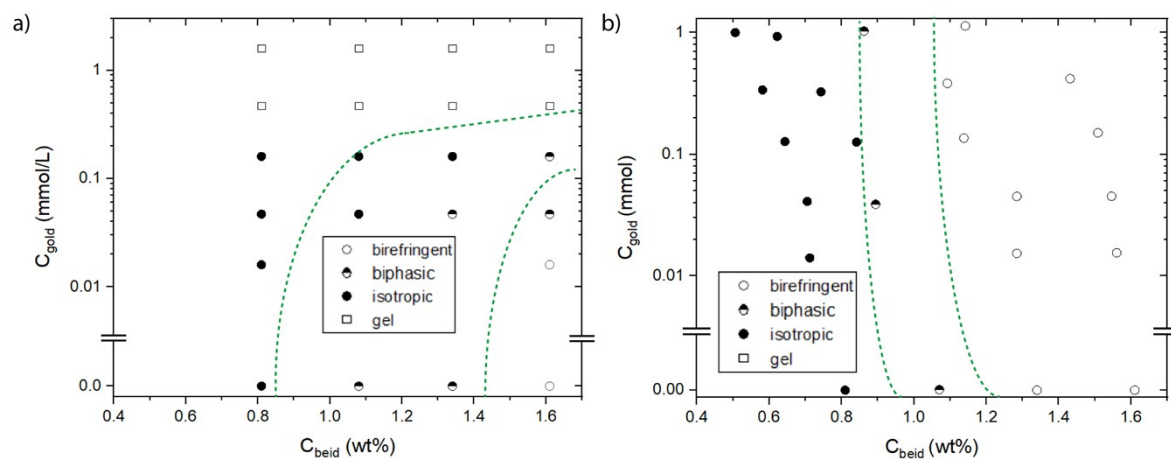
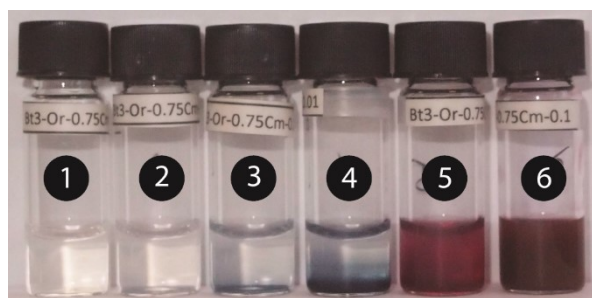
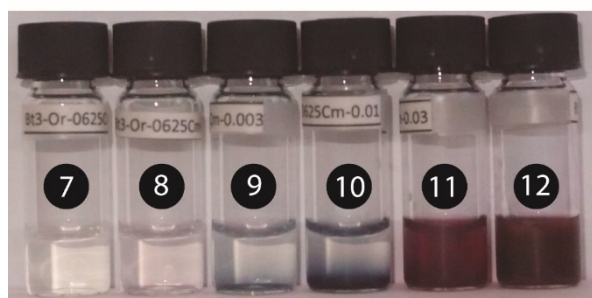


Figure S7. Tentative phase diagrams of the beidellite/gold system. a) just after synthesis; b) after dialysis. Dialysis induced some dilution of the samples, which was accounted for in the corresponding phase diagram. The green dashed lines are only guides to the eye showing the boundaries of the biphasic domain.

## 7. Influence of beidellite concentration



$C_{\text{beid}} = 1.61 \text{ wt } \%$



$C_{\text{beid}} = 1.34 \text{ wt } \%$



$C_{\text{beid}} = 1.07 \text{ wt } \%$



$C_{\text{beid}} = 0.81 \text{ wt } \%$

Figure S8: photographs of beidellite/gold samples observed in natural (left column) and polarized (right column) light, with  $C_{\text{gold}}$  increasing from left to right :  $C_{\text{gold}} = 0, 0.016, 0.047, 0.16, 0.47,$  and  $1.6$  mM, and  $C_{\text{beid}} = 1.61 \text{ wt } \%$  (1<sup>st</sup> row),  $1.34 \text{ wt } \%$  (2<sup>nd</sup> row),  $1.07 \text{ wt } \%$  (3<sup>rd</sup> row), and  $0.81 \text{ wt } \%$  (4<sup>th</sup> row).

The synthesis of gold nanoparticles was achieved in the whole range of beidellite weight fraction,  $C_{\text{beid}}$ , that was explored, from 0.81 to 1.61 wt%. For all values of  $C_{\text{beid}}$ , the blue color was observed for samples with  $C_{\text{gold}} = 0.047$  and 0.16 mM and the purple one for samples with  $C_{\text{gold}} = 0.47$  and 1.6 mM. For all series, a vertical gradient of particle density appeared for samples with  $C_{\text{gold}} = 0.16$  and 0.47 mM, and samples with  $C_{\text{gold}} = 0.47$  and 1.6 mM were gels. As expected, for samples with constant  $C_{\text{gold}}$ , the proportion of nematic phase in the vials decreased with decreasing  $C_{\text{beid}}$ , which is consistent with the 1<sup>st</sup> order character of the isotropic/nematic phase transition.

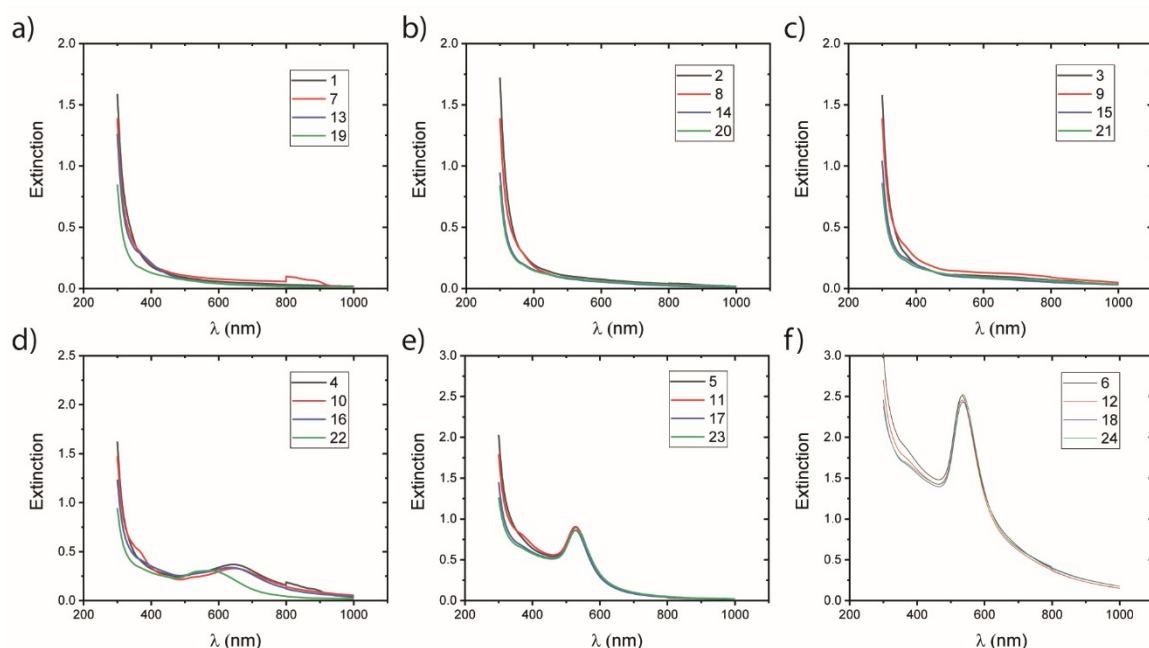


Figure S9: Influence of the variation of  $C_{\text{beid}}$  at constant  $C_{\text{gold}}$  on the UV-vis spectra. a)  $C_{\text{gold}} = 0$  mM; b)  $C_{\text{gold}} = 0.016$  mM; c)  $C_{\text{gold}} = 0.047$  mM; d)  $C_{\text{gold}} = 0.16$  mM; e)  $C_{\text{gold}} = 0.47$  mM; and f)  $C_{\text{gold}} = 1.6$  mM.

We varied  $C_{\text{beid}}$  by a factor of two around the isotropic to nematic phase transition. In this concentration range, at fixed  $C_{\text{gold}}$ , the optical properties of the beidellite/gold nanocomposite colloids do not depend much on  $C_{\text{beid}}$ . Note that beidellite being in large excess ( $20 \text{ g.L}^{-1}$ ) compared with gold (less than  $0.6 \text{ g.L}^{-1}$ ), a relatively small variation of  $C_{\text{beid}}$  should not affect gold nanoparticle synthesis.

## 8. SAXS and WAXS data of beidellite/gold suspensions

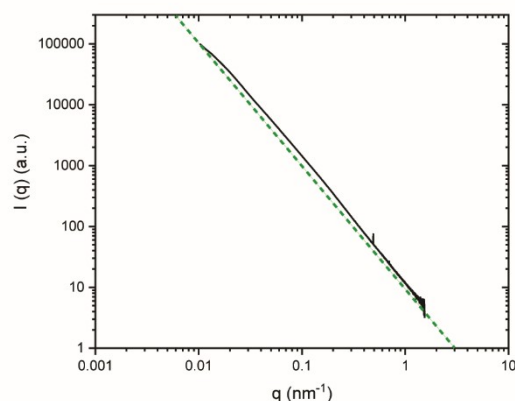


Figure S10: SAXS data of a dilute beidellite/gold suspension. The dashed line shows the  $q^{-2}$  dependence expected for 2-dimensional scattering objects in the intermediate scattering vector range ( $2\pi/d_{\text{beid}} < q < 2\pi/t$ , where  $d_{\text{beid}}$  and  $t$  are respectively the nanosheet diameter and thickness).

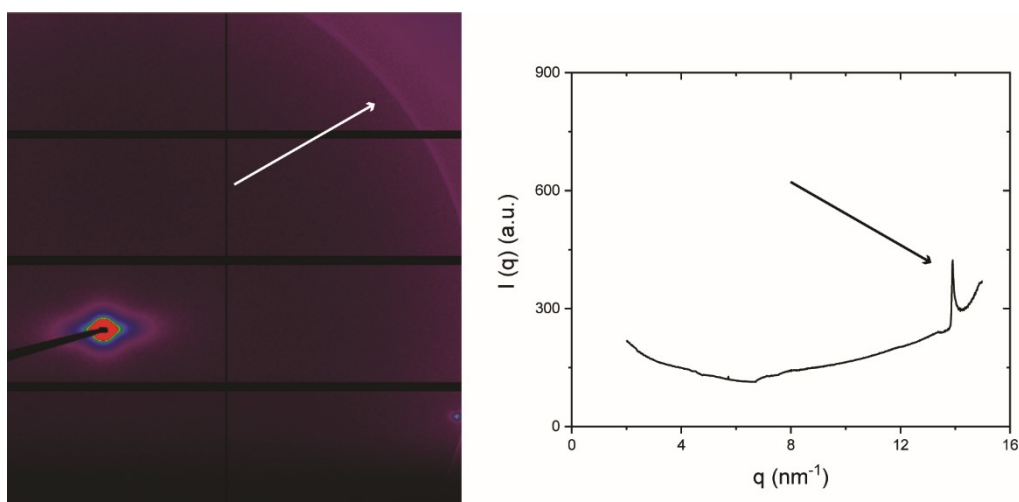


Figure S11: Left: WAXS pattern of a beidellite/gold suspension showing the main diffraction line (white arrow) arising from the internal crystallographic structure of the nanosheets; Right: Corresponding azimuthally-averaged WAXS intensity showing the main reflection (black arrow), with its typical asymmetric profile due to the 2-dimensional nature of the scattering objects.

Altogether, Figures S10 and S11 demonstrate that the nature, size, and internal crystallographic structure of the beidellite nanosheets are preserved after gold nanoparticle growth.

## 9. Influence of an a.c. electric field on a biphasic beidellite/gold suspension

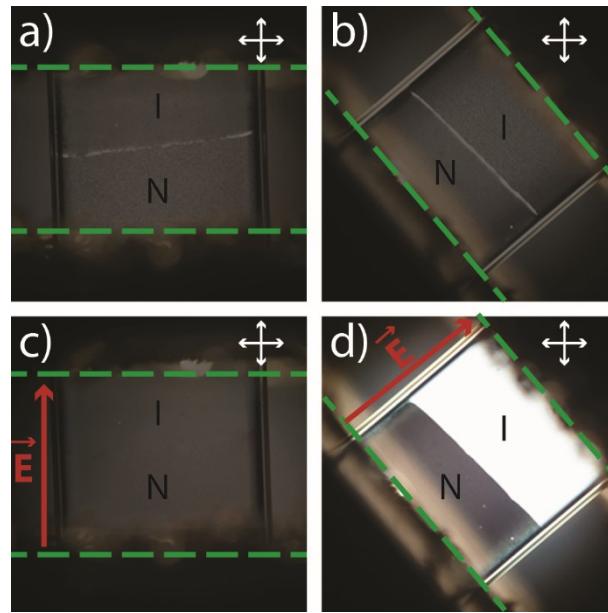


Figure S12: Polarized-light microscopy photographs of biphasic, isotropic (I) / nematic (N), beidellite/gold suspensions held in a 1 mm wide flat glass capillary in the absence of field (a,b) and under an a.c. electric field (red arrow, 500 kHz, 125 V rms). (The green dashed lines show the borders of the electrodes used to apply the field and the white arrows represent the polarizer and analyzer directions.)

Because the isotropic / nematic phase transition is first-order, the regions of stability of these two phases are separated by a biphasic domain in the phase diagram. In this domain, samples left vertical spontaneously demix in the isotropic phase at the top and the denser nematic phase at the bottom (Fig. S12a). The isotropic phase (I) naturally appears dark between crossed polarizers because it is not birefringent. The nematic phase (N) also appears dark in a flat glass capillary because it shows strong “homeotropic” anchoring on the flat glass plates, meaning that the nanosheets lie flat on the plates. Then, the nematic director (revolution symmetry axis of the phase),  $\mathbf{n}$ , is parallel to the direction of light propagation and no birefringence is detected. However, at the I/N interface (faint line separating the I and N regions),  $\mathbf{n}$  lies perpendicular to the interface, which makes it visible between crossed polarizers (Fig. S12b).

In an electric field, the beidellite nanosheets align parallel to the field due to the polarization of their counter-ion clouds (Fig. S12c,d).<sup>1</sup> This actually stabilizes the alignment of the nematic phase which therefore does not change, except that the interface vanishes due to  $\mathbf{n}$  being reoriented by the field in homeotropic alignment. In contrast, the symmetry of the I phase is broken by the application of the field so that it becomes a single-domain birefringent phase (often called paranematic). The

electric field direction is its revolution symmetry axis so that it appears dark when the field is parallel to either the polarizer or the analyzer direction (Fig. S12c) and shows maximum light transmission when the field makes a  $45^\circ$  angle with these directions (Fig. S12d).

1 I. Dozov, E. Paineau, P. Davidson, K. Antonova, C. Baravian, I. Bihannic and L. J. Michot, *J. Phys. Chem. B*, 2011, **115**, 7751–7765.